REPORT DOCUMENTATION PAGE

Form Approved
OMB No. 0704-0188

PLEASE DO NOT RETURN YOUR FORM TO THE ABOVE ORGANIZATION.

1. REPORT DATE *(DD-MM-YYYY)*	2. REPORT TYPE	3. DATES COVERED *(From - To)*
08/10/2010	Final Performance Report	02/01/2007-05/31/2010

4. TITLE AND SUBTITLE
A Hybrid Actuation Approach for Vibration Control of Space Structures

5a. CONTRACT NUMBER
FA9550-07-1-0105

5b. GRANT NUMBER

5c. PROGRAM ELEMENT NUMBER

6. AUTHOR(S)
Ranjan Mukherjee

5d. PROJECT NUMBER

5e. TASK NUMBER

5f. WORK UNIT NUMBER

7. PERFORMING ORGANIZATION NAME(S) AND ADDRESS(ES)

8. PERFORMING ORGANIZATION REPORT NUMBER

9. SPONSORING/MONITORING AGENCY NAME(S) AND ADDRESS(ES)
Air Force Office of Scientific Research
875 North Randolph Street
Arlington, VA22203

10. SPONSOR/MONITOR'S ACRONYM(S)

11. SPONSOR/MONITOR'S REPORT
NUMBER(S) AFRL-OSR-VA-TR-2013-1019

12. DISTRIBUTION/AVAILABILITY STATEMENT
Distribution Statement A: Approved for public release. Distribution is unlimited.

13. SUPPLEMENTARY NOTES

14. ABSTRACT
Our research focused on vibration energy dissipation through sequential application and removal of constraints. With the goal of energy removal from membrane-like structures, we first investigated the problem of a string vibrating against a smooth obstacle. The obstacle is located at one of the boundaries and the string is assumed to wrap and unwrap the obstacle during vibration. The wrapping of the obstacle was modeled by a series of perfectly inelastic collisions and unwrapping was assumed to be energy conserving. The results indicate that the obstacle can be regarded as a passive mechanism for vibration suppression. The energy lost during each cycle of oscillation depends on the energy content of the string at the beginning of the cycle and is greater for higher modes of oscillation. Active vibration control of the string was introduced by applying a displacement constraint at the boundary instead of the obstacle. The state of vibration of the string at the time of constraint application determines if energy is added or removed from the system and this information has been used to develop a new feedback control strategy

15. SUBJECT TERMS

16. SECURITY CLASSIFICATION OF:			17. LIMITATION OF ABSTRACT	18. NUMBER OF PAGES	19a. NAME OF RESPONSIBLE PERSON
a. REPORT	b. ABSTRACT	c. THIS PAGE			19b. TELEPHONE NUMBER *(Include area code)*

A Hybrid Actuation Approach For Vibration Control of Space Structures

AFOSR Contract # FA 9550-07-1-0105

Ranjan Mukherjee, Professor
Department of Mechanical Engineering
Michigan State University
East Lansing, MI 48824-1226
Tel: (517) 355-1834
mukherji@egr.msu.edu

Summary

The objective of this research was to develop vibration suppression strategies for space structures that contain frames and trusses as well as soft elements. Based on our success in earlier work, our initial focus was on cable control of frames and trusses and theoretical and experimental results showed good vibration attenuation through a combination of two distinct effects: a parametric effect that changes structural stiffness and a direct effect that arises due to external forcing. Cable actuators do not lend themselves well to control of soft structures and therefore the latter part of our research focused on a new method of vibration control, where energy redistribution and dissipation would be achieved through sequential application and release of constraints. It was shown that application of constraint typically removes kinetic energy from the system and release of constraint resets the system for a new cycle of constraint application and removal. Conditions that lead to a net loss of kinetic energy per cycle and bounds on the amount of energy removed were examined. The experimental component of this work included energy redistribution in a beam with electromagnetic brakes that were periodically turned on and off; and theoretical extension of the work to soft structures first looked at the problem of passive vibration damping in a string using a obstacle at its boundary. For the string vibration problem, damping can be increased significantly by using a scabbard-like actuator at one boundary but this active method of constraint application and removal can also add energy to the system.

1. Vibration Control of Frames and Trusses Using Cable Actuators:

The numerical model of a structure with cable actuators is developed using finite elements (Issa, et al., 2010), and it takes the form

$$M\ddot{X} + (K - TK_g)X = TF \tag{1}$$

where M and K are the mass and stiffness matrices of the system, F is the external force vector corresponding to unit tension in the cable, X is the vector of nodal displacements and rotations, and K_g is the geometric stiffness matrix corresponding to unit cable tension. The total geometric stiffness effect from cable tension is of the form TK_g since axial loading in the frame elements and the stiffness effects due to the cable elements are both proportional to T. It is useful to express the equations of motion in terms of modal amplitudes η. The model is then truncated to n modes

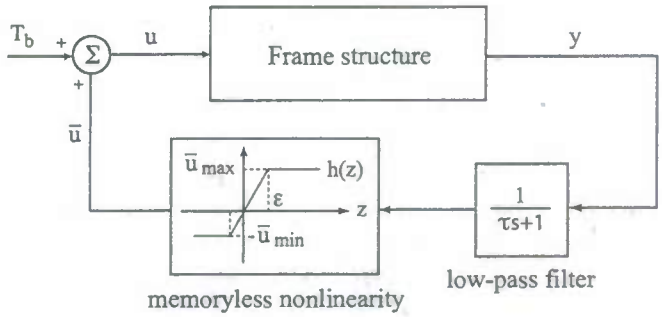

Figure 1. Feedback control design for frame structures

which results in the following equations

$$\ddot{\eta} + \Gamma\dot{\eta} + (\Omega - T\,k_g)\eta = T\,f \tag{2}$$

where k_g is the $n \times n$ modal geometric stiffness matrix and $\Omega = \text{diag}(\omega_i^2)$ is the diagonal matrix of zero-tension natural frequencies. To account for damping, modal damping $\Gamma\dot{\eta}$ is introduced where $\Gamma = \text{diag}(2\xi_i\omega_i)$ is the diagonal modal damping matrix and ξ_i's are the modal damping ratios. In Eq.(2), f is the modal forcing vector. The state space form of Eq.(2) is given by

$$\begin{aligned} \dot{x}_1 &= x_2 \\ \dot{x}_2 &= -\Omega x_1 - \Gamma x_2 + (k_g x_1 + f)u \end{aligned} \tag{3}$$

where $x_1, x_2 \in R^n$ are the modal amplitude and velocity vectors, and tension in the cable is taken to be the input, *i.e.*, $u = T$. We assume the control input to be comprised of a bias tension T_b and an active term $\bar{u}$ that vanishes as the vibrations decay to zero, *i.e.*, $u = \bar{u} + T_b$. The bias tension shifts the equilibrium configuration from $(x_1^T, x_2^T) = (0, 0)$ to $(x_1^T, x_2^T) = (\bar{x}_1, 0)$, where

$$\bar{x}_1 = [\Omega - T_b\,k_g]^{-1}\,f\,T_b \tag{4}$$

where $[\Omega - T_b\,k_g]^{-1}$ exists since T_b is less than the critical buckling load. To shift the equilibrium configuration back to the origin, we define the following transformation of coordinates and input

$$q_1 = (x_1 - \bar{x}_1), \qquad q_2 = x_2, \qquad \bar{u} = u - T_b \tag{5}$$

The state space description in Eq.(3) can now be written as follows

$$\begin{aligned} \dot{q}_1 &= q_2 \\ \dot{q}_2 &= -\Omega q_1 - \Gamma q_2 + [k_g(q_1 + \bar{x}_1) + f]\,\bar{u} + T_b\,k_g\,q_1 \end{aligned} \tag{6}$$

For the system described by Eq.(6), the stability properties of this equilibrium point $(q_1^T, q_2^T) = (0, 0)$ is described with the help of the following theorem:

Theorem 1:
Consider the frame structure modeled by Eq.(6) with bias tension T_b, $T_b > \bar{u}_{min} > 0$. The control design in Fig.1, with the output defined by the relation

$$y = -(q_2^T + q_1^T Q)\,[k_g(q_1 + \bar{x}_1) + f] \tag{7}$$

renders the equilibrium $(q_1^T, q_2^T) = (0, 0)$ asymptotically stable for

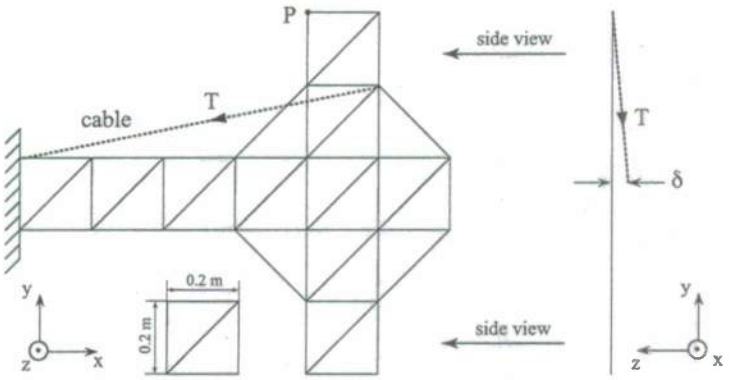

Figure 2. A frame structure

1. any choice of $Q = Q^T \in R^{n\times n}$ which guarantees the positive-definiteness of the two matrices

$$A = \begin{pmatrix} \Omega & Q \\ Q & I \end{pmatrix}, \qquad B = \begin{pmatrix} Q\Omega & \frac{1}{2}Q\Gamma \\ \frac{1}{2}\Gamma Q & \Gamma - Q \end{pmatrix} \tag{8}$$

2. and the bias tension T_b satisfying

$$0 < \bar{u}_{min} < T_b \leq \theta \, \frac{\lambda_{min}(B)}{\lambda_{max}(W)} \tag{9}$$

for $\lambda_{max}(W) > 0$, where $\lambda_{max}(W)$ is the largest eigenvalue of matrix W, defined as

$$W = \begin{pmatrix} Q\, k_g & \frac{1}{2}k_g^T \\ \frac{1}{2}k_g & 0 \end{pmatrix}$$

and $\lambda_{min}(B)$ is the smallest eigenvalue of B and $\theta \in (0,1)$ is any constant.

For numerical simulations, we consider the frame structure model depicted in Fig.2, formed by welding together aluminum bars of circular cross-section of diameter 6 mm and $\delta = 1.0$ mm. The control model utilized the first two modes of the frame, which correspond to first mode bending in the xz plane and simple torsion about the x axis. The natural frequencies of these modes were computed using FEA as $\omega_1 = 7.92$ rad/sec and $\omega_2 = 15.20$ rad/sec, respectively. The damping ratios of these modes were taken to be $\xi_1 = \xi_2 = 0.003$. To ensure positive-definiteness of matrices A and B in Eq.(8), Q was chosen as $Q = 0.0157\,\Gamma$. In accordance with Eq.(9), the bias tension and $\bar{u}_{min}$ were chosen as $T_b = 2\,\bar{u}_{min} = 0.18$ N. For the cable placement shown in Fig.2, the geometric stiffness matrix, the modal forcing vector and the equilibrium configuration were computed (in SI units) and found to be as follows

$$k_g = \begin{pmatrix} 0.326 & 0.319 \\ 0.319 & -0.328 \end{pmatrix}, \quad f = -\begin{pmatrix} 1.13 \\ 1.77 \end{pmatrix} \times 10^{-3}, \quad \bar{x}_1 = -\begin{pmatrix} 0.33 \\ 0.14 \end{pmatrix} \times 10^{-5}$$

Simulation results are shown in Fig.3 for initial conditions $q_1(0) = (0,0)$ and $q_2(0) = (0.12, 0.12)$ in SI units, and control system parameters of $\tau = 1/15$ sec, $\epsilon = 1 \times 10^{-7}$, and $\bar{u}_{max} = 30$ N. It is clear from the plots that the vibration of the modeled modes are very effectively controlled.

Experiments were carried out in the laboratory with a frame similar to the one in Fig.2. The experimental results can be found in the paper by Issa, et al. (2010).

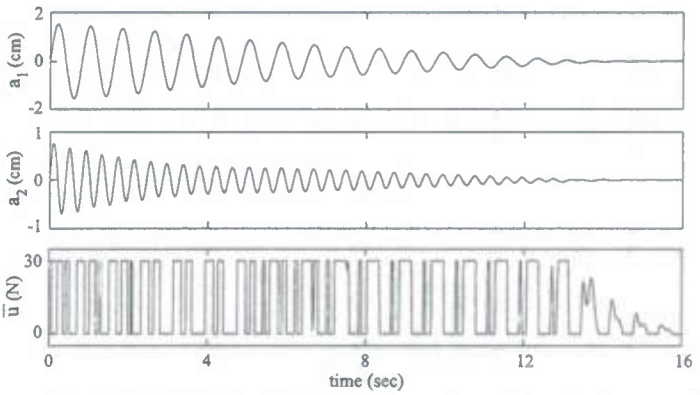

Figure 3. Plot of modal amplitudes $q_1 = (a_1, a_2)^T$ and control effort

2. Energy Dissipation Through Application and Removal of Constraints:

Consider the N-dof linear dynamical system

$$M\ddot{X} + KX = 0 \tag{10}$$

where M and K are the N-dimensional mass and stiffness matrices and $X = [x_1, x_2, \cdots, x_N]^T$ is the vector of independent generalized coordinates. Upon application of a holonomic constraint, the dynamics of the system takes the form

$$\tilde{M}\ddot{Y} + \tilde{K}Y = 0 \tag{11}$$

where $\tilde{M}$ and $\tilde{K}$ are the $(N–1)$-dimensional mass and stiffness matrices and $Y = \left[y_1, y_2, \cdots, y_{(N-1)}\right]^T$ is the vector of independent generalized coordinates of the constrained system.

We denote the unconstrained system as state α and the constrained system as state β. The transition from state α to state β occurs over the brief interval of time when the constraint is applied. If $[t^-_{\alpha\beta}, t^+_{\alpha\beta}]$ denotes this interval, the state transition can be described by the relations

$$\begin{aligned} X(t^+_{\alpha\beta}) &= X(t^-_{\alpha\beta}) && (12)\\ M\dot{X}(t^+_{\alpha\beta}) &= M\dot{X}(t^-_{\alpha\beta}) + I_{\alpha\to\beta} && (13)\\ Y(t^+_{\alpha\beta}) &= T_{\alpha\beta}\, X(t^+_{\alpha\beta}) && (14)\\ \dot{Y}(t^+_{\alpha\beta}) &= T_{\alpha\beta}\, \dot{X}(t^+_{\alpha\beta}) && (15) \end{aligned}$$

where $I_{\alpha\to\beta}$ is the N-dimensional impulse of the generalized forces and $T_{\alpha\beta}$ is a transformation matrix. The transition from state β to state α occurs over a brief interval of time when the constraint is removed. If $[t^-_{\beta\alpha}, t^+_{\beta\alpha}]$ denotes this transition interval, the effect of the transition can be described by the relations

$$\begin{aligned} Y(t^+_{\beta\alpha}) &= Y(t^-_{\beta\alpha}) && (16)\\ \dot{Y}(t^+_{\beta\alpha}) &= \dot{Y}(t^-_{\beta\alpha}) && (17)\\ X(t^+_{\beta\alpha}) &= T_{\beta\alpha} Y(t^+_{\beta\alpha}) && (18)\\ \dot{X}(t^+_{\beta\alpha}) &= T_{\beta\alpha} \dot{Y}(t^+_{\beta\alpha}) && (19) \end{aligned}$$

where $T_{\beta\alpha}$ is a constant and unique transformation matrix. The change in kinetic energy over one

cycle of constraint application and removal is

$$\Delta E = \frac{1}{2}\dot{X}^T(t^+_{\alpha\beta})\, M\, \dot{X}(t^+_{\alpha\beta}) - \frac{1}{2}\dot{X}^T(t^-_{\alpha\beta})\, M\, \dot{X}(t^-_{\alpha\beta}) \tag{20}$$

and through simplifications, it can be shown to be equal to

$$\Delta E = \frac{1}{2}\dot{X}^T(t^-_{\alpha\beta}) I_{\alpha\to\beta} = -\frac{1}{2} I^T_{\alpha\to\beta} M^{-1} I_{\alpha\to\beta} \leq 0 \tag{21}$$

In modal coordinates, the change in kinetic energy can be expressed as follows

$$\begin{aligned} \Delta E &= \tfrac{1}{2}\dot{X}^T(t^-_{\alpha\beta}) M \left[\dot{X}(t^+_{\alpha\beta}) - \dot{X}(t^-_{\alpha\beta})\right] \\ &= \tfrac{1}{2}\dot{\mu}^T(t^-_{\alpha\beta})\Phi^T M \left[\tilde{\Psi}\dot{\nu}(t^+_{\alpha\beta}) - \Phi\dot{\mu}(t^-_{\alpha\beta})\right] \\ &= \tfrac{1}{2}\dot{\mu}^T(t^-_{\alpha\beta})\Phi^T M \left[\tilde{\Psi}\Gamma - \Phi\right]\dot{\mu}(t^-_{\alpha\beta}) \\ &= -\tfrac{1}{2}\dot{\mu}^T(t^-_{\alpha\beta})\Lambda\dot{\mu}(t^-_{\alpha\beta}) \leq 0 \end{aligned} \tag{22}$$

where

$$\Lambda \doteq \left(I_N - \Gamma^T\Gamma\right) \tag{23}$$

$$\Gamma \doteq \tilde{\Psi}^T M \Phi \tag{24}$$

$\Phi = [\phi_1, \phi_2, \cdots, \phi_N] \in R^{N\times N}$ and $\tilde{\Psi} = \left[\tilde{\psi}_1, \tilde{\psi}_2, \cdots, \tilde{\psi}_{(N-1)}\right] \in R^{N\times(N-1)}$ are modal matrices in states α and β, respectively, and I_N is the N-dimensional identity matrix.

To understand the limitations of energy dissipation through application of constraints, consider the matrix $\Gamma^T\Gamma$, where Γ is defined by Eq.(24). It can be shown that $\Gamma^T\Gamma$ is idempotent and hence $\Lambda = \left(I_N - \Gamma^T\Gamma\right)$ is idempotent. The trace of Λ can be computed as

$$\text{trace}[\Lambda] = \text{trace}[I_N] - \text{trace}[\Gamma^T\Gamma] = N - \text{trace}[\Gamma\Gamma^T] = N - \text{trace}[I_{(N-1)}] = 1 \tag{25}$$

From Eq.(25) we deduce that Λ has one unit eigenvalue and other eigenvalues are all zero. If v is the normalized eigenvector of Λ corresponding to its unit eigenvalue, then eigen decomposition of Λ gives

$$\Lambda = vv^T \tag{26}$$

Substitution of Eq.(26) into Eq.(22) gives the expression for the loss in kinetic energy

$$\Delta E = -\frac{1}{2}\dot{\mu}^T(t^-_{\alpha\beta}) vv^T \dot{\mu}(t^-_{\alpha\beta}) = -\frac{1}{2}\left[v^T\dot{\mu}(t^-_{\alpha\beta})\right]^2 \leq 0 \tag{27}$$

It is clear from Eq.(27) that the energy of the system will not be dissipated if any one of the following conditions hold:

1. $\dot{\mu}(t^-_{\alpha\beta}) = 0$: the constraint is applied when the system has zero kinetic energy.
2. $v^T\dot{\mu}(t^-_{\alpha\beta}) = 0$, $v_i \neq 0$, $i = 1, 2, \cdots, N$: the constraint is applied when the modal velocity vector is normal to the eigenvector of Λ corresponding to the unity eigenvalue.
3. $v_i = 0$, $i \in S_r \doteq \{k_1, k_2, \cdots, k_r\}$, $\dot{\mu}_j(t^-_{\alpha\beta}) = 0$, $\forall j \notin S_r$: the kinetic energy of the system lies in specific modes that correspond to zero entries of v.

The first and second conditions can be avoided through a proper choice of time when the constraint is applied. The third condition corresponds to a necessary condition for energy entrapment and can

occur, for example, when the constraint is applied at a node of a system. The sufficient condition for energy entrapment is stated next with the help of the following theorem.

Theorem 1 *The energy of a linear system will remain trapped in r specific modes if Γ contains an orthonormal sub-matrix of dimension r.*

For numerical simulations, consider the system in Fig.4 (Issa, et al., 2009). For this system, Γ, Λ and v were computed as follows:

$$\Gamma^T = \begin{pmatrix} 0.9599 & 0.0 \\ 0.0 & 1.0 \\ -0.2804 & 0.0 \end{pmatrix}, \quad \Lambda = \begin{pmatrix} 0.0786 & 0.0 & 0.2691 \\ 0.0 & 0.0 & 0.0 \\ 0.2691 & 0.0 & 0.9214 \end{pmatrix}, \quad v = \begin{pmatrix} 0.2804 \\ 0.0 \\ 0.9599 \end{pmatrix} \tag{28}$$

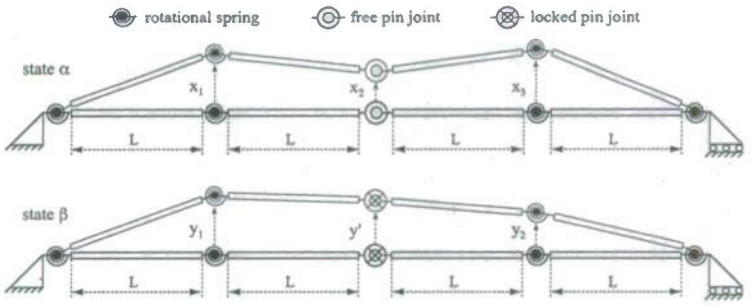

Figure 4. A linear system with 3DOF in state α and 2DOF in state β

From the entries of Γ in Eq.(28) it is clear that the condition in Theorem 1 is satisfied with $r = 1$. Since $\Gamma^T_{2,2} = 1.0$, the energy of the system is trapped in the second mode of state α, which is also the second mode of state β. We can also verify that one element of v, namely v_2, is equal to zero. Energy entrapment can be verified from the simulation results presented in Fig.5, the initial conditions for which were chosen as

$$(x_1, x_2, x_3, \dot{x}_1, \dot{x}_2, \dot{x}_3) = (0.006, 0.016, 0.002, 0.00, 0.00, 0.00)$$

in SI units. In this simulation, the system was switched from state α to state β at the earliest opportunity after 0.2 seconds when the two middle bars are aligned, *i.e.*, when

$$g(X) = x_1 - 2x_2 + x_3 = 0$$

and switched back to state α after 0.2 seconds in state β. The modal amplitudes in state α, namely, μ_1, μ_2, μ_3, are shown in Fig.5 for the intervals of time when the system is in state α. It is clear from these plots that the amplitudes of the first and third modes decay to zero whereas the amplitude of the second mode remains constant. The plot of the energy confirms that some energy of the system gets trapped in the second mode. This is not surprising since the location of the brake at the node of the second mode renders it ineffective.

3. Modal Disparity and its Experimental Verification:

For experimental validation of the work presented in the previous section, we investigated the free vibration of a beam with a mid-span hinge, as shown in Fig.6. Assuming Euler-Bernoulli beam theory, the equation of motion of the beam in the x-y plane can be written as follows

$$EI\, y'''' + m\ddot{y} = 0 \qquad \text{if } x \in (0, L/2) \text{ or } x \in (L/2, L) \tag{29}$$

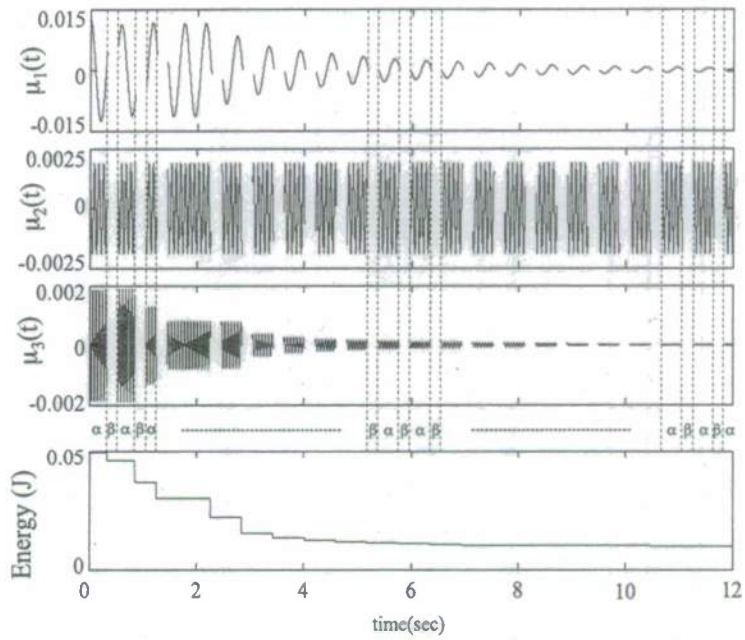

Figure 5. Plot of modal amplitudes in state α and total energy of the system

$$
\begin{aligned}
y(0,t) &= y(L,t) = 0 \\
y^{'}(0,t) &= y^{'}(L,t) = 0 \\
y((L/2)^{-},t) &= y((L/2)^{+},t) \\
y^{'''}((L/2)^{-},t) &= y^{'''}((L/2)^{+},t)
\end{aligned}
$$

and

$$
y^{''}((L/2)^{-},t) = y^{''}((L/2)^{+},t) = 0 \qquad \text{in stiffness state } \alpha\text{: hinge released} \tag{30}
$$

$$
\begin{aligned}
y^{'}((L/2)^{-},t) &= y^{'}((L/2)^{+},t) \\
y^{''}((L/2)^{-},t) &= y^{''}((L/2)^{+},t)
\end{aligned}
\qquad \text{in stiffness state } \beta\text{: hinge locked} \tag{31}
$$

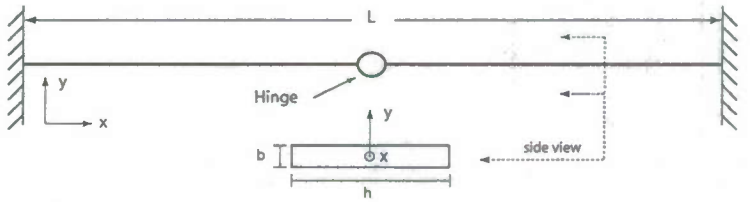

Figure 6. A flexible clamped-clamped beam hinged in the middle

In Eq.(29), E is the modulus of elasticity, I is area moment of inertia, and m is the mass per unit length of the beam. The beam is modeled using N standard (cubic) finite elements, with two degrees of freedom per node (translation and rotation about the z axis). To facilitate the modeling of the hinge in its two states, the node at $x = L/2$ has two rotational degrees of freedom, θ^l and θ^r, corresponding to $y^{'}(L/2^{-},t)$ and $y^{'}(L/2^{+},t)$, respectively. In stiffness state α, the hinge is assumed to be free and θ^l and θ^r are independent. However, in stiffness state β, the hinge is locked and

the constraint $\theta^l = \theta^r$ has to be enforced. This is accomplished by adding a penalty of magnitude $\frac{1}{2}k_r\left(\theta^l - \theta^r\right)^2$ to the strain energy, that is, by adding a rotational stiffness

$$K_r = k_r \begin{bmatrix} 1 & -1 \\ -1 & 1 \end{bmatrix} \tag{32}$$

to the global stiffness matrix. The parameter k_r is set to zero in the stiffness state α and to a large, positive value in stiffness state β. With the additional degree of freedom (in rotation) for the node at $x = L/2$, the finite element model has $(2N-1)$ degrees of freedom.

A lumped mass M is added at the central node to account for the mass of the hinge and the electromagnetic brake. The transition from stiffness state α to stiffness state β is achieved by activating an electromagnetic brake. The activation of the brake occurs over a brief interval of time and results in the application of an action-reaction pair of impulsive moments to the middle node. If $t \in [t^-_{\alpha\beta}, t^+_{\alpha\beta}]$ denotes the activation time, the effect of the impulsive moments can be described by the relations

$$\begin{aligned} Y(t^-_{\alpha\beta}) &= Y(t^+_{\alpha\beta}) \\ M\dot{Y}(t^-_{\alpha\beta}) + I_{\alpha\to\beta} &= M\dot{Y}(t^+_{\alpha\beta}) \end{aligned} \tag{33}$$

where M is the mass matrix and Y is the vector of nodal degrees of freedom. $I_{\alpha\to\beta}$ is the impulse vector with nonzero entries corresponding to the coordinates θ^l and θ^r and has the form

$$I_{\alpha\to\beta} = [0, \cdots, C, -C, \cdots, 0]^T, \qquad C = \int_{t^-_{\alpha\beta}}^{t^+_{\alpha\beta}} \tau(t)\, dt \tag{34}$$

where C is the impulse and τ is the impulsive moment.

The transition from stiffness state β to stiffness state α is achieved by releasing the brake. If $t \in [t^-_{\beta\alpha}, t^+_{\beta\alpha}]$ denotes the brief time interval over which the brake is released, the degrees of freedom and their velocities just prior to and after release of the brake are the same, *i.e.*

$$Y(t^-_{\beta\alpha}) = Y(t^+_{\beta\alpha}), \qquad \dot{Y}(t^-_{\beta\alpha}) = \dot{Y}(t^+_{\beta\alpha}) \tag{35}$$

With this notation, the stiffness parameter k_r can be defined as follows

$$k_r = \begin{cases} 0 & \text{stiffness state } \alpha \\ k_\infty & \text{stiffness state } \beta \end{cases}$$

where k_∞ is some large positive number chosen to enforce the constraint $\theta^l = \theta^r$.

Consider the clamped-clamped beam in Fig.6 with the following properties:

Table 1. Material and geometric properties of clamped-clamped beam in Fig.6

Material	Aluminum
Young's Modulus	71 GPa
Density	2710 Kg/m^3
Dimensions	$2.0 \times 0.05 \times 0.0023$ m
Hinge mass	0.182 Kg

The natural frequencies of the first four modes of the beam in the two stiffness states are shown in Table 2. Since the hinge is located at mid-span, the natural frequencies of even numbered modes in

the two stiffness states are identical. This is true because even-numbered modes have zero curvature at mid-span and are not affected by the state of the hinge, *i.e.* locked or released. The first four mode shapes of the beam in the two stiffness states are provided in Fig.7 for reference.

Table 2. Natural frequencies of the finite element model of the beam in the two stiffness states

$\omega_{\alpha i}$, $\omega_{\beta i}$ (rad/sec)		mode number, i			
		$i=1$	$i=2$	$i=3$	$i=4$
stiffness state	α	1.29	8.34	9.52	27.0
	β	2.30	8.34	14.68	27.0

Using modal truncation, the matrix measure of modal disparity was computed using the first four modes as follows

$$\Psi^T M \Phi = \begin{pmatrix} 0.980 & 0.000 & 0.153 & 0.000 \\ 0.000 & 1.000 & 0.000 & 0.000 \\ 0.139 & 0.000 & 0.949 & 0.000 \\ 0.000 & 0.000 & 0.000 & 1.000 \end{pmatrix} \tag{36}$$

The second and fourth rows and columns of the matrix in Eq.(36) maintain the identity structure. This is indicative of the fact that even-numbered modes in the two stiffness states are identical. The nonzero elements in the off-diagnonal entries of the matrix are indicative of the presence of modal disparity between the two stiffness states and indicate how modal energy will be redistributed between odd-numbered modes in these two states.

Consider the scenario where the beam is initially in stiffness state α and vibrating purely in the third mode with an amplitude A. The total energy of the beam is equal to $E_\alpha = 0.5\, A^2\, \omega_{\alpha 3}^2$. It is assumed that there is no damping in the system and that the brake is activated when the beam passes through its neutral position. The modal velocities in stiffness states β can be computed as

$$\begin{bmatrix} \dot{\nu}_1(t^+_{\alpha\beta}) \\ \dot{\nu}_2(t^+_{\alpha\beta}) \\ \dot{\nu}_3(t^+_{\alpha\beta}) \\ \dot{\nu}_4(t^+_{\alpha\beta}) \end{bmatrix} = \begin{pmatrix} 0.980 & 0.000 & 0.153 & 0.000 \\ 0.000 & 1.000 & 0.000 & 0.000 \\ 0.139 & 0.000 & 0.949 & 0.000 \\ 0.000 & 0.000 & 0.000 & 1.000 \end{pmatrix} \begin{bmatrix} 0 \\ 0 \\ A\,\omega_{\alpha 3} \\ 0 \end{bmatrix} \tag{37}$$

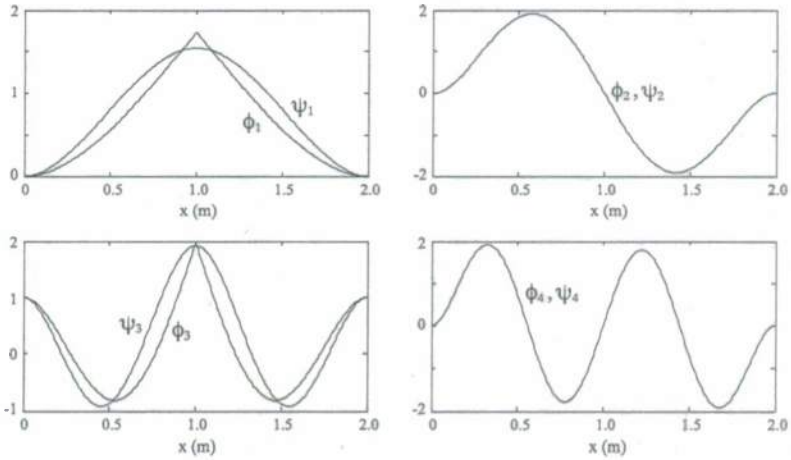

Figure 7. Mode shapes of the clamped-clamped beam in the two stiffness states

Clearly, the energy of the beam is redistributed in modes 1 and 3 in stiffness state β. The amount of energy in these modes are

$$E_{\beta 1} = \frac{1}{2} 0.153^2 A^2 \omega_{\alpha 3}^2 = 0.153^2 E_\alpha, \qquad E_{\beta 2} = \frac{1}{2} 0.949^2 A^2 \omega_{\alpha 3}^2 = 0.949^2 E_\alpha \tag{38}$$

It can be easily shown that the amplitudes of these modes are $0.153A(\omega_{\alpha 3}/\omega_{\beta 1}) = 0.633A$ and $0.949A(\omega_{\alpha 3}/\omega_{\beta 3}) = 0.615A$, respectively. These results have been validated through experiments. A description of the experimental setup can be found in the paper by Issa, et al., (2008).

4. Vibration of a String Wrapping/Unwrapping an Obstacle in its Boundary:

Consider a string vibrating against an obstacle placed at one of its boundaries, as shown in Fig.8. We investigate energy dissipation in the string under the following assumptions:

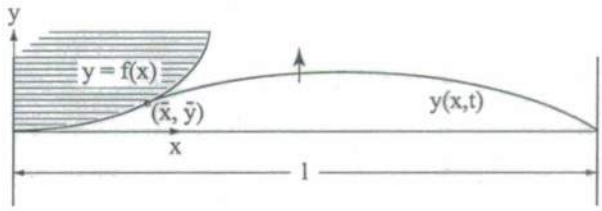

Figure 8. A string vibrating against an obstacle.

A1. The obstacle is rigid and has the following geometry

$$y = f(x), \qquad y(0) = 0, \quad \left[\frac{dy}{dx}\right]_{x=0} = 0 \tag{39}$$

A2. The string is homogenous and has a constant mass per unit length denoted by ρ. The tension in the string is equal to T and remains constant at all times. The string undergoes transverse vibration in the xy plane and is not affected by gravity.

A3. The amplitude of oscillation of the string is small and therefore the equation of motion of the string can be expressed by the standard relation

$$\left(\frac{\partial^2 y}{\partial x^2}\right) = \frac{1}{c^2}\left(\frac{\partial^2 y}{\partial t^2}\right), \qquad c \triangleq \sqrt{T/\rho} \tag{40}$$

where $y(x,t)$ is the displacement of the string at a distance x from the origin at time t.

A4. The string wraps around the obstacle during vibration. Over each time step during wrapping, a small element of the string comes to rest on the obstacle through perfectly inelastic collisions. The wrapping process continues till the freely vibrating portion of the string has no more kinetic energy.

A5. The surface of the obstacle is not sticky and the string unwraps from the obstacle without any loss of energy.

A6. At the initial time $t = 0$, the string has no contact with the obstacle. It is in its mean position with zero potential energy and kinetic energy equal to E_0.

A7. The string continues to vibrate in the mode in which it started its vibration at the initial time. This implies that each point of the string, not in contact with the obstacle, has the same frequency of vibration at any instant of time, and the number of nodes in the vibrating string remains constant.

A8. The string has no internal damping, *i.e.*, the energy of the string will remain conserved during free vibration.

A general solution to the partial differential equation in Eq.(39) can be written as

$$y(x,t) = A\,(\sin\lambda x - \tan\lambda l\,\cos\lambda x)\,\sin\omega t \tag{41}$$

We now consider the boundary conditions at the contact break point. From Fig.10 we have

$$f(\bar{x}) = y(\bar{x},t) \qquad \Longrightarrow \qquad f(\bar{x}) = A\,(\sin\lambda\bar{x} - \tan\lambda l\,\cos\lambda\bar{x})\,\sin\omega t \tag{42}$$

Also, the string is tangential to the obstacle at the contact break point $x = \bar{x}$, *i.e.*,

$$f'(\bar{x}) = \frac{\partial y}{\partial x}(\bar{x},t) \qquad \Longrightarrow \qquad f'(\bar{x}) = \lambda A\,(\cos\lambda\bar{x} + \tan\lambda l\,\sin\lambda\bar{x})\,\sin\omega t \tag{43}$$

From Eqs.(42) and (43) we get

$$\tan\lambda(l-\bar{x}) = -\lambda\frac{f(\bar{x})}{f'(\bar{x})} \tag{44}$$

which indicates that λ can be computed from the value of $\bar{x}$. The solution of Eq.(44) is however not unique - each non-trivial value of λ corresponds to a mode of vibration of the string.

Let the total energy of the string at any time t be denoted by E. Then,

$$E = E_{\text{pe}} + E_{\text{ke}} = E_{\text{pe}}^{\text{obs}} + E_{\text{pe}}^{\text{vib}} + E_{\text{ke}} \tag{45}$$

where $E_{\text{pe}}^{\text{obs}}$ is the potential energy of the string wrapped around the obstacle, $E_{\text{pe}}^{\text{vib}}$ is the potential energy of the freely vibrating string, E_{pe} is the total potential energy, and E_{ke} is the kinetic energy of the string. The total potential energy of the string is computed as the product of the tension T and elongation of the string

$$E_{\text{pe}} = T\int dl = T\int(ds - dx) = T\int(\sqrt{dx^2+dy^2} - dx) = T\int_0^l(\sqrt{1+(dy/dx)^2} - 1)dx$$

and $E_{\text{pe}}^{\text{obs}}$ and $E_{\text{pe}}^{\text{vib}}$ can be written as

$$E_{\text{pe}}^{\text{obs}} = T\int_0^{\bar{x}}(\sqrt{1+(dy/dx)^2} - 1)dx, \qquad E_{\text{pe}}^{\text{vib}} = T\int_{\bar{x}}^l(\sqrt{1+(dy/dx)^2} - 1)dx$$

Since the string conforms to the shape of the obstacle, $(dy/dx) = f'(x)$ for $x \in [0,\bar{x}]$. By expressing $(dy/dx) = y'(x,t)$ for $x \in [\bar{x},l]$ and simplifying, we get

$$E_{\text{pe}}^{\text{obs}} = T\int_0^{\bar{x}}\left[\sqrt{1+[f'(x)]^2} - 1\right]dx \tag{46}$$

$$E_{\text{pe}}^{\text{vib}} = T\int_{\bar{x}}^l\left[\sqrt{1+[y'(x,t)]^2} - 1\right]dx = \frac{1}{8}T\lambda\sec^2\lambda l\Big\{2\lambda(l-\bar{x}) + \sin[2\lambda(l-\bar{x})]\Big\}\left[g(\bar{x})\right]^2 \tag{47}$$

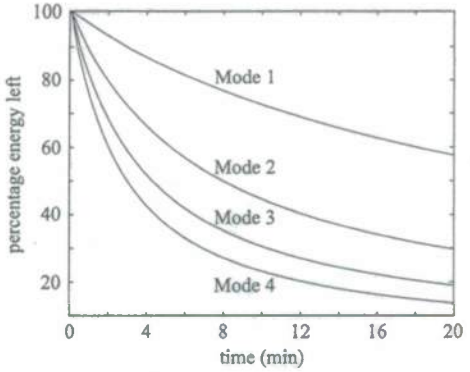

Figure 9. Exponential decay in the energy of a string wrapping and unwrapping around an obstacle. The plots show energy decay for single-mode vibration in the first four modes with $E_0 = 0.5\ J$.

where $g(\bar{x})$ is defined in Alsahlani and Mukherjee (2010(a)). The kinetic energy of the vibrating string can be written and simplified as follows

$$E_{\text{ke}} = \frac{1}{2}\int_{\bar{x}}^{l} \rho[\dot{y}(x,t)]^2 dx = \frac{1}{8\lambda}\rho\omega^2 \sec^2\lambda l\Big\{2\lambda(l-\bar{x}) - \sin[2\lambda(l-\bar{x})]\Big\}\Big\{A^2 - [g(\bar{x})]^2\Big\} \tag{48}$$

From the above equations it is easy to verify that the energy expression has the form

$$E = h(\bar{x}, A) \tag{49}$$

For a configuration in which the string is wrapped around the obstacle, the complete solution can be determined from the values of $\bar{x}$ and E using the four-step algorithm described in Alsahlani and Mukherjee (2010(a)).

For numerical simulations, consider a string with

$$T = 1\text{ N}, \qquad \rho = 0.025\text{ kg/m}, \qquad l = 4\text{ m} \tag{50}$$

The obstacle is assumed to be a circle of radius R and center coordinates $(x, y) \equiv (0, R)$, *i.e.*,

$$y = f(x) = R - \sqrt{R^2 - x^2}, \qquad 0 \le x \le R \tag{51}$$

Figure 9 plots the decay in energy as a function of time for vibration in the first four modes with $E_0 = 0.5\ J$. The following observations can be made:

For any mode of oscillation, it can be seen that the percentage energy loss is higher for higher values of E_0. This is not surprising since higher values of E_0 results in higher kinetic energy and greater length of wrapping, as evident from the values of $\bar{x}_k$ in Table 3, and consequently more energy loss through inelastic collision.

The percentage energy loss is higher for higher modes of oscillation for the same value of E_0. This is true for the same number of cycles as well as for the same length of time and is due to the fact that the velocities of the string associated with higher frequencies are higher in higher modes, and as a consequence the loss upon impact is higher. The value of $\bar{x}_k$ is less for the higher modes but this does not have a significant effect on percentage of energy loss.

5. Vibration Control of a String Using a Scabbard-Like Actuator:

Consider the vibrating string in Fig.10(a), that passes through a scabbard located at its left boundary. At time $t = t_c$, the scabbard is moved instantaneously to the right by distance x_0 along the mean position of the string. This is shown in Fig.10(b). At some future time $t = t_r$, $t_r > t_c$, the scabbard is moved back to its original position. To investigate the effect of application and removal of the scabbard on the vibration of the string, we assume that the movement of the scabbard imposes a zero-displacement constraint over the length interval $x \in [0, x_0)$. The displacement and velocity of the string over the remaining interval $x \in [x_0, l]$ remains unchanged immediately after movement of the scabbard. Additionally, at time $t = t_r$, $t_r > t_c$, the scabbard is instantaneously moved back to its original position, *i.e.*, to the left by a distance x_0 along the mean position of the string. The displacement and velocity of the string over the interval $x \in [x_0, l]$ remains unchanged immediately after movement of the scabbard.

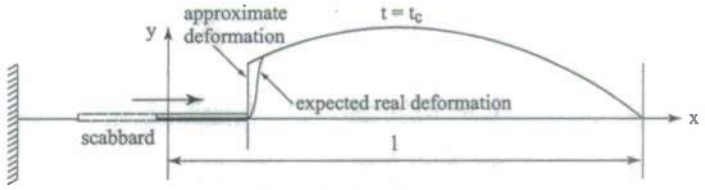

Figure 10. A zero-displacement constraint is applied to the string at time $t = t_c$ over the length segment $x \in [0, x_0)$ using a scabbard.

We skip the mathematical development here which can be found in Alsahlani and Mukherjee (2010(b)) and present simulation results for one cycle of constraint application and removal.

We consider a string of length $l = 4$ m, mass per unit length $\rho = 0.25$ kg/m, and tension $T = 1$ N, vibrating in its first mode with unit amplitude $A_0 = 1$ m. At $t = 0$ the string is assumed to pass through its mean position, and the equation of motion of the string is

$$y_0(x,t) = \sin(\frac{\pi}{4}x)\,\sin(\frac{\pi}{2}t) \tag{52}$$

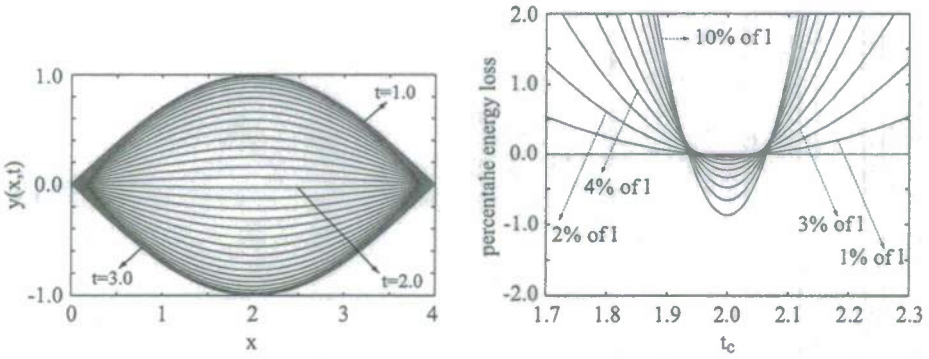

Figure 11. (a) Position of the string at different time instants (b) Percentage change in energy of the string due to application of the constraint for different values of x_0 and t_c.

The time period of oscillation of the string is 4 sec and Fig.11(a) shows the shape of the string at different instants of time over the interval $t \in [1.0, 3.0]$ sec. The string has maximum potential energy at $t = 1.0$ sec and $t = 3.0$ sec, and maximum kinetic energy at $t = 2.0$ sec.

We present simulation results for percentage change in energy due to constraint application for $x_0 \in \{0.0l, 0.01l, 0.02l, \cdots, 0.09l, 0.10l\}$ and $t_c \in [1.7, 2.3]$ sec. The results, shown in Fig.11(b),

indicate that the energy of the string increases if the constraint is applied when the string is far away from the mean position, and decreases if the constraint is applied when the string is near its mean position, irrespective of the value of x_0. Upon application of the constraint, the potential energy of the string increases. This increase is large when the string is far away from its mean position, and although the constraint removes the kinetic energy of a portion of the string, there is a net gain in energy. When the string is near its mean position, the increase in energy due to change in potential energy is small compared to the loss of kinetic energy and as a result the net change in energy is negative. When the string is at its mean position, there is no change in potential energy upon application of the constraint and consequently the energy loss is maximum in this configuration. For the same value of t_c, a larger value of x_0 results in a larger increase in potential energy and a larger decrease in kinetic energy.

We have investigated the effect of application of the constraint on the dynamics of the string with arbitrary initial conditions such that sequential application and removal of constraints can be explored as a strategy for vibration suppression - see Alsahlani and Mukherjee (2010).

Publications Resulting from the AFOSR Contract:

Journal Publications

[1] Issa, J., Mukherjee, R., Diaz, A. R., and Shaw, S. W., 2008, "Modal Disparity and its Experimental Verification", *Journal of Sound and Vibration*, Vol.311, Nos.3-5, pp.1465-1475.

[2] Issa, J., Mukherjee, R., and Diaz, A. R., 2009, "Energy Dissipation in Dynamical Systems Through Sequential Application and Removal of Constraints", *ASME Journal of Dynamic Systems, Measurement and Control*, Vol.131, No.2.

[3] Alsahlani, A. and Mukherjee, R., 2010(a), "Vibration of a String Wrapping and Unwrapping an Obstacle", *Journal of Sound and Vibration*, Vol.329, pp.2707-2715, 03/2010.

[4] Issa, J., Mukherjee, R., and Shaw, S. W., 2010, "Vibration Suppression in Structures Using Cable Actuators", *ASME Journal of Vibration and Acoustics*, Vol.132.

[5] Alsahlani, A. and Mukherjee, R., 2010(b), "Vibration Control of a String Using a Scabbard-Like Actuator", *Journal of Sound and Vibration* (submitted).

Conference Publications

[1] Issa. J., Mukherjee, R., and Shaw, S. W., "Control of Space Structures Using Cable Actuators", *ASME Dynamic Systems and Control Conference (DSCC)*, Ann Arbor, MI, 2008.

[2] Issa. J., Mukherjee, R., and Diaz, A. R., "Energy Dissipation through Modal Energy Redistribution", *ASME Dynamic Systems and Control Conference (DSCC)*, Ann Arbor, MI, 2008

[3] Issa. J., Mukherjee, R., and Diaz, A. R., "Energy Removal in Dynamic Systems through an Optimal Sequence of Constraint Application", *ASME Dynamic Systems and Control Conference (DSCC)*, Ann Arbor, MI, 2008.

[4] Issa, J., Mukherjee, R., and Diaz, A. R., "Vibration Suppression in Space Structures through Cyclic Application and Removal of Constraints", *50th AIAA Structures, Structural Dynamics and Materials Conference*, Palm Springs, CA, 2009.

[5] Alsahlani, A., and Mukherjee, R, "Dynamics and Energetics of a String Vibrating Against an Obstacle Placed at a Boundary", *ASME International Design Engineering and Technical Conference (IDETC)*, Montreal, Canada, 2010.

[6] Alsahlani, A., and Mukherjee, R, "Suppression of String Vibration Using a Constraint Actuator at One Boundary, *ASME International Design Engineering and Technical Conference (IDETC)*, Montreal, Canada, 2010.

PhD Dissertation Research Supported by the AFOSR Contract:

Jimmy Issa, currently Assistant Professor at Lebanese American University, ByBlos, Lebanon
Dissertation Title: *Vibration Suppression Through Stiffness Variation and Modal Disparity*
Department of Mechanical Engineering, Michigan State University, June 2008.

Since July 2008, the contract funded the dissertation research of another PhD student who is expected to graduate by 2012.